2023

Influence of Thermal Cycling on Degradation Behavior of Thermal Greases

P. P. Nagrani

R. V. Kulkarni

A. M. Marconnet

Nagrani, P. P.; Kulkarni, R. V.; and Marconnet, A. M., "Influence of Thermal Cycling on Degradation Behavior of Thermal Greases" (2023). *CTRC Research Publications.* Paper 423.
http://dx.doi.org/https://doi.org/10.1109/ITherm55368.2023.10177495

2023 22nd IEEE Intersociety Conference on Thermal and Thermomechanical Phenomena in Electronic Systems (ITherm) | 979-8-3503-2166-1/23/$31.00 ©2023 IEEE | DOI: 10.1109/ITHERM55368.2023.10177495

Influence of Thermal Cycling on Degradation Behavior of Thermal Greases

Pranay P. Nagrani
School of Mechanical Engineering
Purdue University
West Lafayette, IN, USA
pnagrani@purdue.edu

Ritwik V. Kulkarni
School of Mechanical Engineering
Purdue University
West Lafayette, IN, USA
kulka103@purdue.edu

Amy M. Marconnet
School of Mechanical Engineering
Purdue University
West Lafayette, IN, USA
marconnet@purdue.edu

***Abstract*—Thermal management of electronic devices has been an ongoing challenge in the semiconductor industry owing to the increasing power density. The bottleneck of thermal resistance between the device and the heat sink solution is often interfaces between two different substrates. These substrates also often have different coefficient of thermal expansion (CTE). Therefore, a thermal grease is generally employed to reduce the overall thermal resistance. But the performance of thermal grease often worsens with time due to the thermomechanical cycling driven by the CTE mismatch between the substrates. This leads to degradation of thermal greases, which increases the interface resistance and the junction temperatures. In this study, we isolate the effect of thermal cycling (from the mechanical cycling) on degradation of two thermal greases: DOWSIL 340 heat sink compound and DOWSIL TC-5622 thermally conductive compound, by subjecting them to temperature cycling between 20 °C to 100 °C with a cycling frequency of 30 minutes per cycle while holding the bond line thickness constant. We perform a parametric study at different bond line thicknesses (BLTs) of 23 μm, 59 μm, and 84 μm. Before testing the grease, a set of heat loss calibration experiments are performed to enable quantitative evaluation of the grease thermal performance. In addition to thermocouples in the system, we leverage high resolution temperature mapping of the thermal grease using an infrared (IR) microscope for evaluation of local degradation. Specifically, we sandwich the thermal grease (dot dispense) between a ceramic heater and calcium fluoride wafer (due to its IR transparency) to resolve the temperature maps at the top surface of thermal grease. Further, the thermal resistance, void fraction, and area of thermal grease are measured at 24 hour intervals to monitor the degradation performance *in situ*. We observe outward radial movement in DOWSIL-340 (*i.e.*, increase in thermal grease area) and crack formations at thick BLT in early stages of thermal cycling, while at the thin BLT, the degradation is primarily observed at the circumference of the grease. Further, no degradation is observed in DOWSIL-5622 at all three BLTs. We hypothesize this is due to its stable and repeatable viscosity variation with temperature cycling. These results demonstrate a pathway for evaluating thermal grease performance by showcasing importance on the viscosity-temperature hysteresis. This in-turn forms a stepping stone to characterize the coupled thermo-mechanical degradation of thermal greases.**

***Index Terms*—thermal grease, coefficient of thermal expansion, void fraction, infrared, thermal cycling**

I. Introduction

Miniaturization of electronic packages has lead to increased power densities [1]–[3] necessitating effective thermal management solutions to ensure reliability of electronic products. However for heat to be dissipated effectively by the cooling solution, it has to first pass through multiple interfaces and, hence, a thermal interface material (TIM) is used to connect components. Typically thermal greases fill the microscopic air pockets and provide high thermal conductivity pathways between two surfaces to enhance heat transfer, while offering mechanical compliance compared to other types of TIMs (*e.g.*, solders) [4].

Degradation of thermal greases is a long-standing problem [5]–[8]. Specifically, over repeated cycles of use, thermal greases fail via pump-out (movement of thermal grease) and dry-out (separation of polymer matrix), which eventually leads to unacceptable junction level temperatures. Thus, a variety of test protocols have been developed to understand the failure mechanisms of thermal greases [9]. A few studies have concentrated on the influence of thermal cycling on thermal grease degradation [8], [10], [11] by stacking the grease between substrates with high CTE mismatch. Due to long degradation periods in application, accelerated tests can be used to evaluate thermal grease degradation based on mechanical cycling (*e.g.*, [12]). Mechanical cycling simulates the cyclic die warpage when the device is repeatedly powered to fixed level. In these types of studies, temperature can be monitored during cycling (and generally increases as the cycling progresses), but the underlying mechanism of degradation (the pump-out behavior) is generally evaluated only *after* the cycling concludes. One qualitative study by Nnebe and Feger [13] observed dry-out in thermal greases and attributed to changes in the thermal grease microstructure. Specifically, they observed that a drainage network is formed when greases are exposed to thermal cycling and oscillations causing the polymer matrix to escape and air to penetrate causing phase separation. Gowda *et al.* [14] subjected thermal grease to high temperatures and pressures observed the formation of voids resulting in increasing thermal resistance. The influence of matrix type (silicone vs. non-silicone oil) on thermal grease degradation was studied by Carlton *et al.* [15] by subjecting them to mechanical cycling at two different temperatures: 50 °C and 80 °C. They observed enhanced degradation of silicone oil based grease at higher strains due to lower viscosity compared to the non-silicone oil based counterpart. Overall, these past works investigate the thermo-mechanical degradation of thermal grease *after* the

degradation. The present work focuses on isolating the impact of thermal cycling on thermal grease degradation *during* the degradation process.

We subject the thermal greases to power cycling such that junction level temperatures are oscillated between $20\ ^{\circ}\mathrm{C}$ to $100\ ^{\circ}\mathrm{C}$. The bondline is fixed during cycling to isolate the effect of thermal degradation from thermo-mechanical degradation (often due to mismatched CTE) seen in a constant pressure systems. We perform infrared (IR) microscopy to study the 2D in-plane temperature variation across the top surface of the thermal grease. The temperature maps are complemented with black and white (B&W) images to understand the degradation patterns. Finally, we quantify the thermal grease performance by comparing normalized area, void fraction, and area normalized thermal resistance.

II. Experimental Methods

This section overviews the experimental test fixture, calibration experiments, testing procedure, image analysis techniques, and measurement of viscosity.

A. Test Fixture

An experimental setup was built in-house to study the influence of thermal cycling on thermal grease degradation at a fixed BLT while allowing *in situ* thermal imaging. As shown in Fig. 1 a ceramic heater (from WATLOW) of $15\ \mathrm{mm} \times 15\ \mathrm{mm}$ surface area is placed in a machined pocket in a block of Teflon insulation to hold it rigidly. The thermal grease is dispensed on top of heater surface with the help of a $5\ \mathrm{mm}$ diameter circular stencil to ensure a neat, uniform, void-free and consistent dispense pattern. Two plastic shims placed at the edge of heater maintain the desired BLT when the thermal grease is squeezed by the IR-transparent $15\ \mathrm{mm} \times 15\ \mathrm{mm} \times 0.5\ \mathrm{mm}$ calcium fluoride wafer/window (which allows for thermal imaging). To ensure flat, parallel contact between the heater and the wafer and to minimize the likelihood of the wafer of cracking, an aluminum protective clamp (with an open center zone to allow IR imaging) is placed on top of the calcium fluoride wafer and pressed down with approximately equal spring compression force. In order to maximize heat transfer through the thermal grease-CaF_2 wafer path, an inclined fan (from WINSINN) blows air at the center of the calcium fluoride wafer. Representative temperatures of heater surface, clamp edge, and bottom of Teflon insulation are measured with T-type thermocouples (from OMEGA). The temperature measurements enable measurement of the thermal resistance of thermal grease. The IR microscope captures the radiance and temperature maps of the top surface of the thermal grease by imaging through the calcium fluoride wafer.

B. Thermal Cycling Parameters

The thermal cycling is carried out for 4 days at a cycling period of $30\ \mathrm{mins}$ and 50% duty cycle (that is $15\ \mathrm{mins}$ of heating and cooling periods). We limit the testing time to 4 days due to long nature of tests and to facilitate comparison of results. Thermal images are taken initially after the first power cycle at day 0 and then at 24 hour intervals. In addition, the steady state thermal resistance of the thermal grease are also calculated from the measured thermocouple temperatures to quantify the overall performance. Two different thermal greases (DOWSIL-5622 and DOWSIL-340) are tested for thermal degradation by subjecting them to thermal cycling at three different BLTs: $23\ \mu\mathrm{m}, 59\ \mu\mathrm{m}$, and $84\ \mu\mathrm{m}$.

C. Estimation of Thermal Grease Thermal Resistance

The thermal resistance of the thermal grease is calculated from the measured data in a multi-step process based on the input heater power (Q_{input}) and the measured thermocouple temperatures at the heater (T_{heater}), bottom of the Teflon (T_{bottom}), the clamp (T_{clamp}), and the ambient environment (T_{∞}).

Based on the measured data during an experiment, we could find the total thermal resistance from the heater to the environment ($R_{total} = (T_{heater} - T_{\infty})/Q_{input}$), but this would include contributions both from the thermal grease pathway and the pathway through the Teflon insulation. Thus, we first calibrate for the thermal resistance of the loss pathway through the Teflon (R_{loss}, see Section II-C1 for details). This enables calculation of the portion of the heat transferred through the thermal grease as $Q_{thru} = Q_{input} - Q_{loss}$, where $Q_{loss} = (T_{heater} - T_{\infty})/R_{loss}$.

Then, we quantify the total thermal resistance from the heater to the aluminum clamp through the thermal grease: R_{hc}, based on evaluation of $(T_{heater} - T_{clamp})$ and Q_{thru}. To estimate the portion of this resistance due to the thermal grease itself, we need to first quantify the thermal resistance of the calcium fluoride wafer and top aluminum clamp (R_{wc}, see Section II-C2 for details). Then, we can determine the thermal grease thermal resistance as: $R_{grease} = R_{hc} - R_{wc}$.

1) Heat Loss through the Teflon Insulation Pathway: To quantitatively evaluate the thermal resistance of the thermal grease, heat loss through the Teflon insulation must first be calibrated. This is required in order to estimate the heat flow through the thermal grease (needed to calculate thermal resistance) from the total heater power and heater temperature (refer Fig. II-A and Fig. 2). For the calibration experiment, a previously characterized silicone pad insulation (thermal conductivity = $0.14 \pm 0.01\ \mathrm{Wm^{-1}K^{-1}}$) (refer to Appendix C for detailed description about the cross-plane thermal conductivity characterization) is placed on top of heater surface and temperatures are measured on top of silicone pad insulation (T_{top}) and bottom of Teflon insulation (T_{bottom}) using T-type thermocouples in addition to heater temperature measurement (T_{heater}) as shown in Fig. 2. A 1D heat transfer assumption was made in order to characterize the unknown Resistance of the Teflon: R_{PTFE}. Steady state (heater temperature variation less than $1\ ^{\circ}\mathrm{C}$ in 10 mins) values were obtained at six different power levels in order to characterize the thermal resistance through the Teflon insulation to ambient. The total resistance in the loss pathway is the sum of the the conduction resistance through the Teflon and any conduction/convection to ambient ($R_{loss} = R_{PTFE} + R_{ambient,bottom}$).

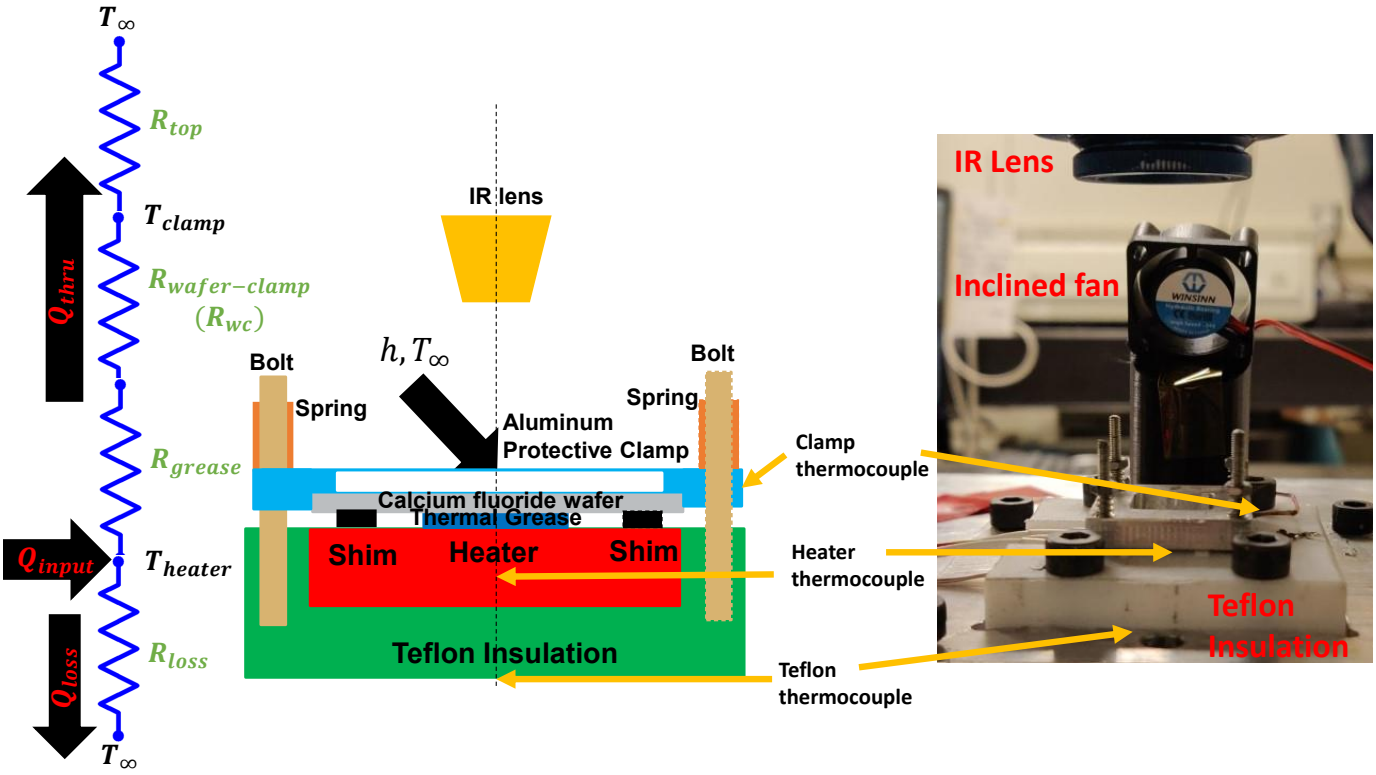

Fig. 1: (Left) 1D thermal resistor network. (Middle) Schematic of thermal cycling text fixture and (right) experimental prototype of thermal cycling test fixture. During thermal cycling, the heat generated at the heater flows through the thermal grease or is lost through the teflon insulation. A forced convection inclined air cooling is employed to maximize the heat transfer through the thermal grease. Temperatures are measured at the heater surface, aluminum clamp and bottom of teflon insulation by using thermocouples. A high resolution IR microscope is used to map the 2D temperature field at the top surface of thermal grease.

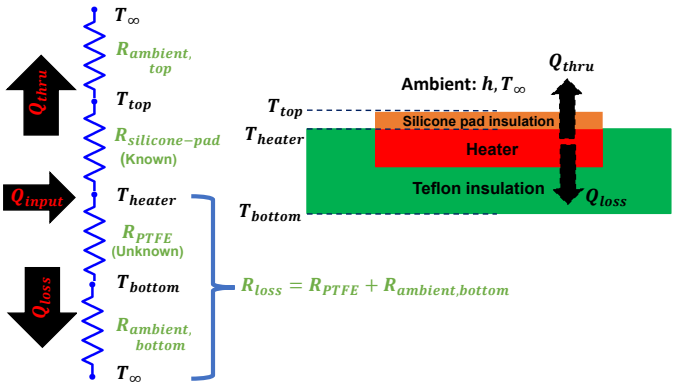

Fig. 2: (Left) One-dimensional thermal resistance network and (right) schematic of the experiment for calibrating heat loss through the Teflon insulation. The total heater power either conducts through the Teflon insulation (Q_{loss}) or through the Silicone pad of known thermal properties ($Q_{silicone-pad}$). Thermocouple measurements at the heater (T_{heater}), top surface of the Silicone pad (T_{top}), and bottom of the Teflon insulation (T_{bottom}) enable identification of the thermal resistance of the Teflon (R_{loss}) given the previously characterized $R_{silicone-pad}$.

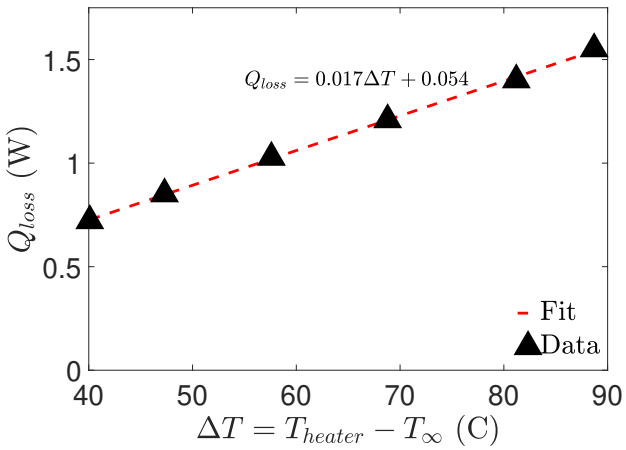

Fig. 3: Heat loss through the Teflon insulation as a function of the temperature difference between the heater and the ambient temperature (T_∞) at different power levels to obtain the total thermal resistance of loss pathway through the Teflon: $R_{loss} = 1/(0.017\ \mathrm{W/K}) = 59.6 \pm 2.3\ \mathrm{K/W}$.

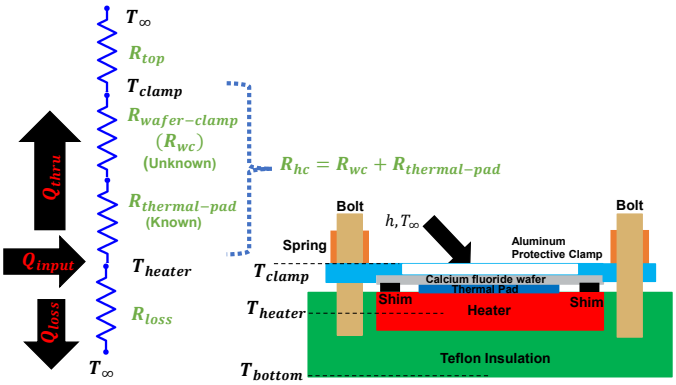

Fig. 4: (Left) One-dimensional thermal resistance network and (right) schematic of the experiment to calibrate the resistance of the calcium fluoride wafer and aluminum clamp. A thermal pad with known thermal resistance is sandwiched between the heater and the calcium fluoride window. Temperatures are measured with thermocouples at the heater (T_{heater}), bottom of the Teflon (T_{bottom}), a representative location on the clamp (T_{clamp}), and the ambient air temperature (T_∞).

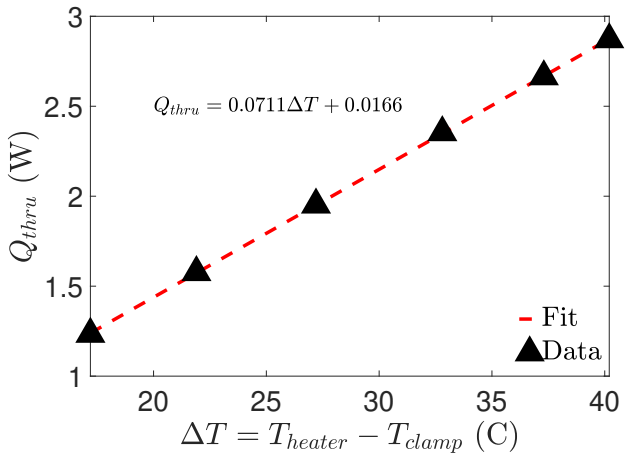

Fig. 5: Heat through the stack as a function of temperature difference at different power levels to obtain $R_{hc} = 1/0.0711 = 14.06 \pm 0.14$ K/W.

For a given heat input, first the heat flow through silicone pad insulation is calculated from $Q_{silicone-pad} = (T_{heater} - T_{top})/R_{silicone-pad}$. Next, the heat loss from Teflon insulation is characterized by subtracting the heat flow through silicone pad from the input heat in the system: $Q_{loss} = Q_{input} - Q_{silicone-pad}$. Finally, a linear curve was fit to the heat loss (via Teflon insulation) as a function of the temperature difference ($T_{heater} - T_\infty$) as shown in Fig. 3 to find the total thermal resistance through the Teflon insulation pathway as $R_{loss} = 1/(0.017 \text{ W/K}) = 59.6 \pm 2.3$ K/W.

2) Calibration of the Calcium Fluoride Wafer - Aluminum Clamp Thermal Resistance: To later enable characterization of the thermal resistance of the thermal grease, we need to calibrate the thermal resistance of the calcium fluoride wafer and aluminum clamp as shown in Fig. 4. An Arctic Blue thermal pad of known thermal resistance and uniform surface properties is sandwiched between the heater and the calcium fluoride wafer. The thermal conductivity of the thermal pad is $k_{pad} = 1.23 \pm 0.05$ $\text{Wm}^{-1}\text{K}^{-1}$ and thermal resistance $R_{thermal-pad} = 7.29$ KW^{-1}. Refer to Appendix C for detailed description about the cross-plane thermal conductivity characterization. Heat transfer is approximated to be 1D for this calibration.

We measure the temperature of heater (T_{heater}) and clamp (T_{clamp}) using thermocouples to obtain the heater-clamp thermal resistance as $R_{hc} = (T_{heater} - T_{clamp})/Q_{thru}$, where R_{hc} is the total heater-clamp thermal resistance (including the (known) resistance of the thermal pad ($R_{thermal-pad}$) and the unknown wafer-clamp resistance ($R_{wafer-clamp}$)) and Q_{thru} is the heat passing through the thermal pad. The heat loss through the Teflon to ambient pathway is calculated by $Q_{loss} = (T_{heater} - T_\infty)/R_{loss}$, where R_{loss} is previously calibrated. Thus, the heat transfer through the thermal pad can be calculated from: $Q_{thru} = Q_{input} - Q_{loss}$.

Six steady state readings are taken and Q_{thru} is linear with the temperature difference $T_{heater} - T_{clamp}$, as shown in Fig. 5. A linear fitting enables calculation of the total thermal resistance from the heater to the path as the inverse of slope: $R_{hc} = 1/(0.0711 \text{ W/K}) = 14.06 \pm 0.14$ K/W

Finally, using the thermal resistance network (Fig. 4), the thermal resistance of calcium fluoride wafer and aluminum clamp (R_{wc}) is obtained as $R_{wc} = R_{hc} - R_{thermal-pad} = 6.78 \pm 0.4$ K/W. This calibration will enable to us to calculate R_{grease} in the degradation experiments with thermal grease.

D. Infrared Imaging

1) Calibration of Thermal Images: For accurate measurements of temperature with infrared imaging, the emissivity must be calibrated. Typically this is accomplished by heating the system to a uniform and known temperature, recording a IR radiance image, and comparing to the radiance from a blackbody at the same temperature. Since the thermal grease moves during cycling, the emissivity map is not constant throughout thermal cycling. Evaluating of the thermal grease *ex situ* on a thermal stage illustrated the thermal grease emissivity is approximately uniform, but varies with BLT perhaps due to slight transmissivity of the grease.

Thus, the IR images and temperature maps reported in this work are taken by assuming a constant thermal grease emissivity (characterized separately at each BLT) for the entire system (grease and heater surface) that is imaged. The effect of thermal cycling causes dynamic movements of the thermal grease in the form of voids and radial outward movement which causes the heater surface to be exposed (or covered) to the IR lens resulting in nonphysical temperatures in the exposed heater regions (due to incorrect emissivity values) which had thermal grease initially. Hence the temperature maps represented in Section III are qualitative and no actual temperature values are reported here.

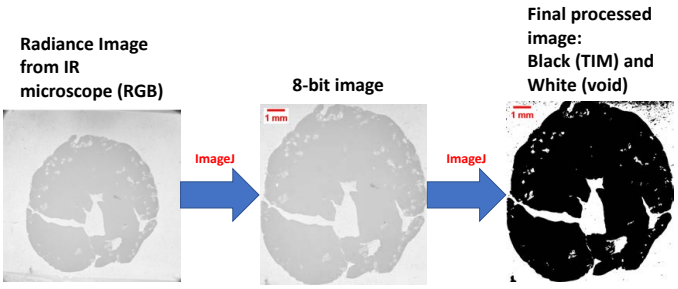

Fig. 6: Workflow of image processing to obtain high quality black and white images of the thermal grease. The radiance data from the IR microscope (left) are processed in ImageJ into 8-bit images (center) and then thresholded (also in ImageJ) to yield the black and white images (right). The black zones are the thermal grease and the white zones are the void space.

2) Image Processing & Analysis: We obtain a radiance image from the IR microscope (during each day of imaging) which is processed in imageJ [16] to measure the area covered by thermal grease and void fraction. As shown in Fig. 6, the radiance image from IR microscope (RGB image originally) is converted to 8-bit image and boundary of the thermal grease is identified manually. The field of view (FOV) of IR lens is known apriori and is used to define the scale bar in the 8-bit converted radiance image. Next, a default threshold is performed in imageJ [16] to obtain a B&W image (Black region - thermal grease, white region - ceramic heater). Finally, the area of grease coverage and void fraction can be calculated from the B&W image.

E. Evaluation of Viscosity

To complement the pumpout experiments, the evolution of the viscosity with temperature over several cycles is evaluated with an Anton-Paar TwinDrive MCR 702 rheometer (Couette cell type rheometer). The thermal grease is subjected to a constant low shear rate of $1/s$ while the temperature is ramped up (and down) from 25 °C to 100 °C (and 100 °C to 25 °C) over a period of 15 mins each in a linear fashion. The time period for the test was 30 mins which matches the time period of the pump-out experiments performed above and test was performed for 8 hours (which we think is enough time to enable us to understand thermal grease degradation behavior).

III. Results and Discussion

In this section, we show the degradation behavior of thermal greases when subjected to thermal cycling followed by performance quantification. Finally, we investigate the temperature dependent viscosity profiles of the thermal greases to explain the degradation behavior.

A. Influence of Thermal Cycling

Figure 7 shows the processed B&W images complemented with thermal maps (from IR microscope) at different days

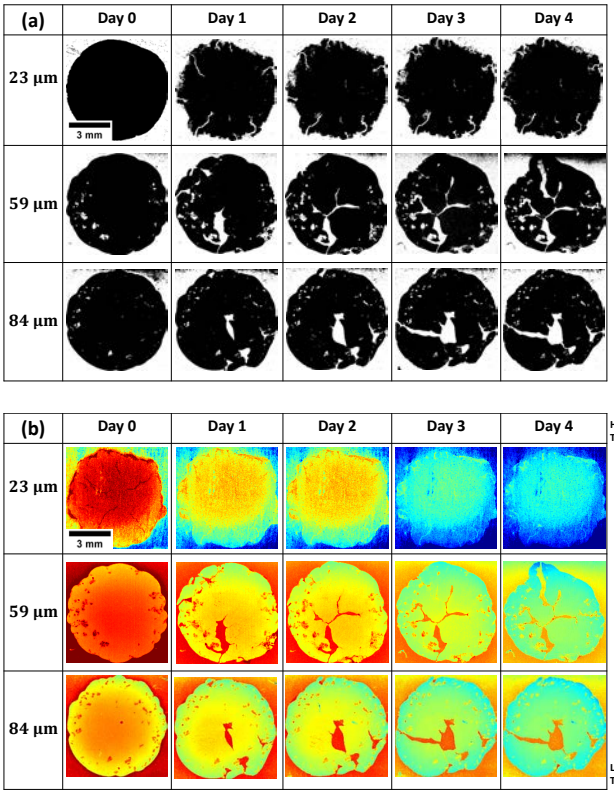

Fig. 7: (a) Processed B&W images and (b) qualitative temperature maps of DOWSIL-340 throughout cycling. Note, the scale bar in top left image applies to all images. The B&W images and temperature maps highlight the void propagation at higher BLTs and void suppression at lower BLTs in DOWSIL-340 due to temperature cycling.

of thermal cycling at three different BLTs for DOWSIL-340. There is pump out (outward radial movement of grease) and void formation when thermally cycled. The void formation shows dendrite type structures at higher BLTs of 59 μm and 84 μm where voids are able to propagate through the grease, on the other than at 23 μm, the initial void formation at the circumference of the grease are not able to propagate through the grease indicating better performance (*i.e.*, lesser degradation). It must be noted that images at day 0 were taken after the first power cycle and hence the voids at 59 μm and 84 μm form in the first power cycle itself.

On the other hand, DOWSIL-5622 shows no degradation in the 4 days of cycling at all BLTs, as shown in Fig. 8. The thermal grease retains its shape and form through out the cycling period indicating minimal impact of thermal cycling on the pump-out.

B. Relation between Thermal Cycling and Temperature-Dependent Viscosity

Contrasting behavior of the two grease under consideration may be explained by studying the variation of thermal grease viscosity with temperature ramp up and down as shown

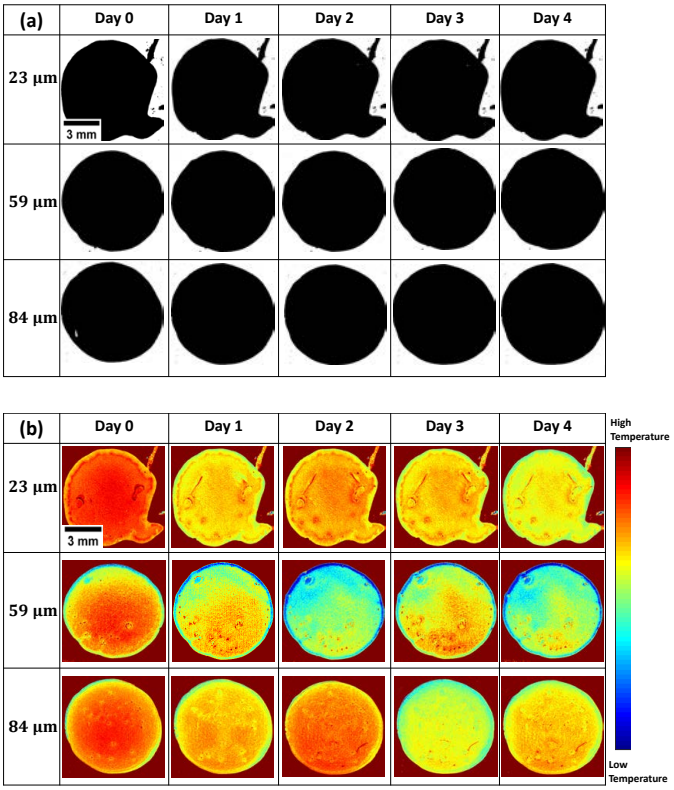

Fig. 8: (a) Processed B&W images and (b) qualitative temperature maps of DOWSIL-5622 throughout cycling. Note, the scale bar in top left image applies to all images. The B&W images and temperature maps highlight no degradation in DOWSIL-5622 due to temperature cycling.

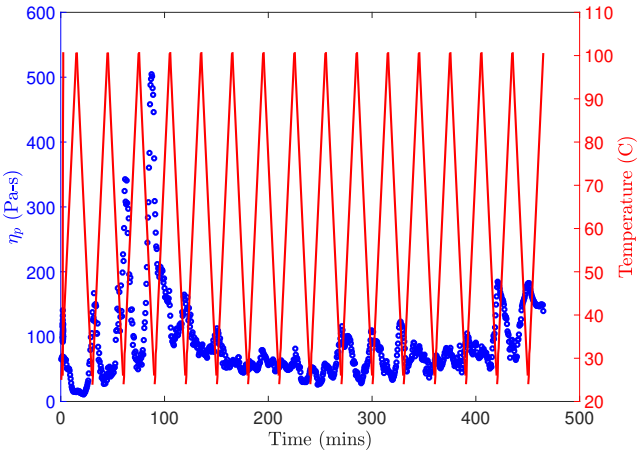

(a)

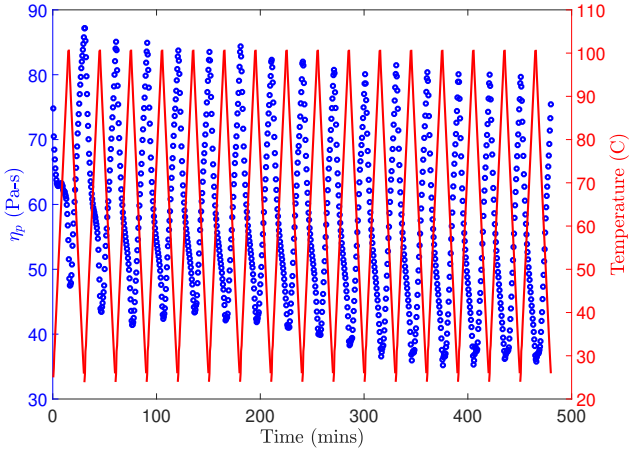

(b)

Fig. 9: Impact of temperature ramping and cycling on the viscosity of (a) DOWSIL-340 and (b) DOWSIL-5622 thermal greases. The results for DOWSIL-340 are non-repeatable and vary rather arbitrarily with repeated cycling, while the results for DOWSIL-5622 are more consistent from cycle to cycle.

in Fig. 9. Due to the fixed BLT, we expect that only the temperature dependent viscosity is predominant factor for motivating or prohibiting pump-out (*i.e.*, mechanical stresses are negligible and do not contribute to pump-out).

As seen from Fig. 9a, for DOWSIL-340 the viscosity variation with temperature is non-repeatable and arbitrary. A very large increase in viscosity followed by sharp decrease is observed in the third temperature cycle indicating micro-structure breakdown. This enables the movement and void formation of DOWSIL-340 observed before in thermal cycling experiments (Fig. 7). At higher BLTs, due to larger temperature drop, the relative viscosity variation within the grease BLT is high causing relative movement amongst different 2D layers of thermal grease which causes void formation [9], [12].

In contrast to the DOWSIL-340, DOWSIL-5622 shows repeatable and stable viscosity variation due to temperature cycling (see Fig. 9b). Within each cycle of heating the viscosity decreases with increasing temperature, then increases as temperature decreases. There is a slight overall decrease in viscosity over time indicating stable micro-structure and hence no degradation was seen in Fig. 8.

Our results suggest that the magnitude of viscosity itself is not indicative of the thermal grease pump out, rather the temperature dependent viscosity impacts the thermal degradation.

C. Performance Quantification

In this subsection, we compare the performance of thermal greases under consideration by monitoring the:

- Normalized Thermal Resistance: R''/R''_o, where $R'' = R_{grease}/A_{grease}$ and R''_o is area normalized resistance at day 0
- Normalized Area: A/A_o, where A_o is area at day 0, and
- Void fraction (ϕ)

over different days of thermal cycling.

The area at each day is quantified by the outer perimeter of the thermal grease and include both area filled by the grease and the voids that form within the perimeter. As seen in Fig. 10a, initially the thermal grease expands slighlty with larger radial spreading is observed in DOWSIL-340 compared

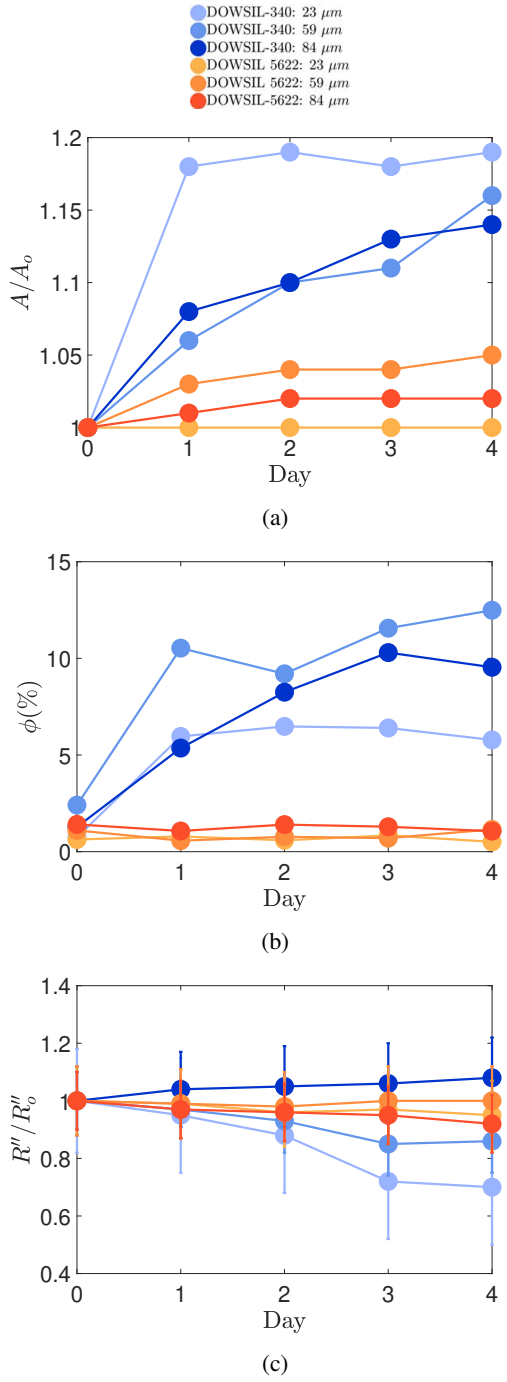

Fig. 10: Evolution of (a) normalized area, (b) void fraction and (c) area normalized thermal resistance with days of thermal cycling. The normalized area shows enhanced radial spreading for in DOWSIL-340, while movement in the DOWSIL-5622 is suppressed. Similarly, more voids form in DOWSIL-340 than in DOWSIL-5622. The area normalized thermal resistance is relatively constant because of the constant volume of grease within the test setup during cycling. That is, although the grease moves, it does not leave the interface between the heater and the heat sink clamp.

to DOWSIL-5622 (from day 0 to day 1). After the first day of cycling, the area covered by both thermal grease remains approximately constant. In addition, a larger percentage of area increase is observed in the lowest BLT (23 μm) test, which may be due to the thin bondline requiring more area change for the same volume change. The larger increase in DOWSIL-340 area (compared to DOWSIL-5622) is likely due to sudden plummet of DOWSIL-340 viscosity during the cooling cycle causing easy outward radial movement. In DOWSIL-5622, the viscosity drop is limited and gradual causing reduced movement of the grease.

Next, Fig. 10b shows the evolution of the void fraction present within the boundary of the thermal grease. More voids indicate larger heater regions which are exposed to air, where thermal grease was present earlier. DOWSIL-5622 showed negligible degradation and void formation (Fig. 8) and, hence, the void fraction is consistently less than 0.5%. In contrast, DOWSIL-340 showed significant degradation. For DOWSIL-340 (Fig. 10b), a large fraction of the voids form in the first day of cycling, after which voids progress more slowly. Voids appear to propagate more easily through the thermal grease at higher BLTs (59 μm and 84 μm) resulting in a larger void fraction at higher BLTs.

Finally, the area normalized thermal resistance (see Fig. 10c) remains approximately constant at $R''/R''_o = 1$ for most of the tests. For DOWSIL-340 at smaller BLTs (23 μm and 59 μm), the resistance slightly reduces to 0.6 and 0.8, respectively. Note that the uncertainty in this estimation of R'' is sufficiently large and hence these variations are not statistically significant. Due to the small dot-shaped dispense of thermal grease compared to the size of the heater, while thermal cycling causes formation of voids and outward radial movement of the thermal grease, there is no actual material loss from the interface (*i.e.*, all of the thermal grease remains in the gap between the heater and the clamp, only its configuration changes with time). Due to this conservation of thermal grease in the interface, the junction level heater temperature and clamp temperature are almost constant (within uncertainty bounds) across all the days of thermal cycling. Thus, the area normalized thermal resistance is approximately constant (within the uncertainty bounds).

IV. Conclusion

In this paper, we observe degradation of thermal greases driven by thermal cycling using a combination of analysis techniques. We isolate the influence of thermal cycling (as opposed to thermo-mechanical cycling) on the thermal grease degradation (*in-situ*) by fixing the BLTs: 23 μm, 59 μm and 84 μm so that mechanical stresses are negligible. We perform thermal cycle test (for 4 days) on DOWSIL-340 and DOWSIL-5622 by subjecting them to cycling temperature variations between 20 °C to 100 °C, and observe that the temperature dependent viscosity could be the predominant effect to drive pump-out. For DOWSIL-340, we observed significant formation of voids and large radial movement.

The void formation exposes heater surface which was previously covered with thermal grease generating areas of local temperature hot-spots. Most of the structural change in the DOWSIL-340 (area increase and void formation) happened during the first day of cycling. The voids were seen to more easily propagate through the grease at higher BLTs. At lower BLTs, the voids were limited at the circumference of DOWSIL-340. Enhanced degradation at higher BLTs may be due to the larger temperature drop across the interface causing large viscosity variation within the thermal grease and, hence, relative motion of different layers of DOWSIL-340. On the other hand, DOWSIL-5622 showed negligible degradation over the 4 days of thermal cycling.

The contrasting behaviors of thermal grease degradation can be justified by tracking the viscosity variation with temperature cycling. In DOWSIL-340, unrepeatable and arbitrary viscosity variation was observed when temperature was ramped up and down (25 °C to 100 °C and vice-versa) indicating broken microstructure within the thermal grease, which could explain the degradation due to thermal cycling. In contrast, DOWSIL-5622 showed consistent and repeatable viscosity variation over 8 temperature cycles indicating in tact microstructure and, hence, more resistance to thermal degradation.

Given these results, an interesting pathway for future work is to study the behavior of DOWSIL-5622 in presence of thermal and mechanical stresses by keeping the pressure on thermal grease to be constant (instead of BLT). Further, showing actual material loss due to pump-out would be interesting to understand the evolution of area normalized thermal resistance.

ACKNOWLEDGMENT

Financial support for this work provided by members of the Cooling Technologies Research Center, a graduated National Science Foundation Industry/University Cooperative Research Center at Purdue University, is gratefully acknowledged.

We thank Prof. Kendra Erk and members of Soft Material Mechanics group at Purdue University for insightful discussions and assistance with performing experiments in Anton Paar MCR-702 rheometer.

We thank Prof. Ivan Christov for helpful discussions regarding the impact of viscosity and temperature-dependent viscosity on pump-out.

APPENDIX A: EXPERIMENT REPEATABILITY

In this section we repeat thermal cycling experiment for the DOWSIL-340 thermal grease at 59 μm BLT. This test condition was selected to repeat as significant void propagation and radial spreading was observed in the initial experiments (Fig. 7). The experimental conditions and assembly were kept the same and the grease was subjected to thermal cycling for 4 days. The processed B&W images are shown in Fig. 11 where Expt. 1 is the original experimental data shown in the main text (Fig. 7) and Expt. 2 is the repeated experiment.

Similar to the initial test, we observe in Expt. 2 that majority of voids form during the first day of cycling. Moreover, the voids propagate through the thermal grease in both experiments indicating enhanced degradation with repeated cycling. Although the void pattern is different, the dendritic pattern and progression of the voids are comparable. Hence, it can be concluded that the degradation behavior observed in thermal grease due to thermal cycling is sufficiently repeatable.

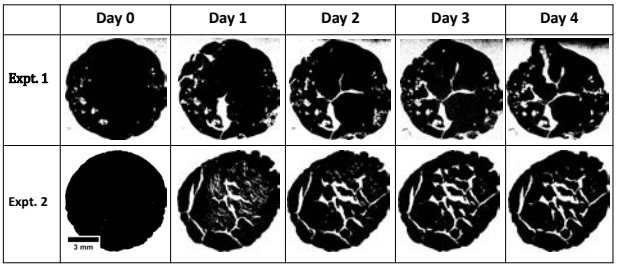

Fig. 11: Repeatability experiment for DOWSIL-340 at 59 μm BLT. Expt. 1 corresponds to original experiment in Fig. 7 and Expt. 2 corresponds to the repeated experiment

APPENDIX B: LEVERAGING IR MICROSCOPY TO OBSERVE VOID FORMATION

We leverage high resolution IR microscope from QFI (Quantum Focus Instruments) to capture a video of void formation in DOWSIL-340 at 84 μm as shown in Fig. 12 (where $t^* = t/t_{end}$ is non-dimensional time). Since emissivity is a strong function of temperature, we use two-temperature emissivity calibration method to calibrate the thermal grease emissivity. Two radiance maps are taken at approximately 20 °C and 100 °C (temperature bounds of thermal cycling) and emissivity is interpolated in the intermediate temperatures.

The two-temperature emissivity calibration is done during the beginning of day 1 and, hence, both voids and grease present at that time are depicted at a relatively uniform temperature (green color) in top-left subfigure of Fig. 12. Due to dynamic thermal grease movement (*i.e.*, void formation and outward radial movement), the IR microscope highlights the void formation and outward grease movement due to the now incorrect emissivity in those regions. The original pixels which had been assigned the emissivity of DOWSIL-340 now image the ceramic heater directly when a void is formed and, hence, the temperature is over estimated (these pixels appear orange instead of green). Next, when DOWSIL-340 moves radially outwards, the original pixels which had emissivity of ceramic heater now image the DOWSIL-340 resulting in an underestimation of temperature (change in color from green to blue).

This is essentially automatic image subtraction within the IR microscope software and can highlight the progression of the thermal grease movement and void formation.

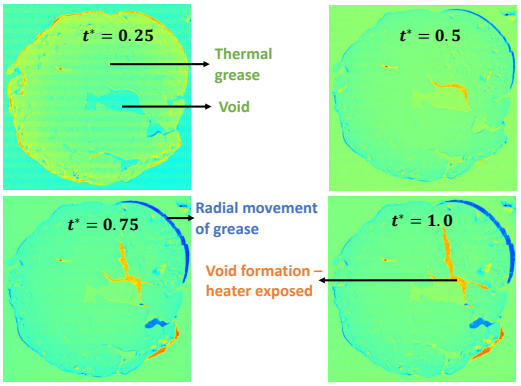

Fig. 12: Void formation and radial DOWSIL-340 movement observed in IR microscopy using a spatially-calibrated emissivity map. The time stamp, $t^* = t/t_{end}$, is non-dimensional time where t_{end} is the time at which last frame in video was captured. The blue regions indicate zones where when calibrated the system viewed the ceramic heater, but after thermal cycling the heater is covered with thermal grease (resulting in an underestimation of temperature). The orange and red regions indicate regions where void have formed in the thermal grease (resulting in an overestimation of temperature).

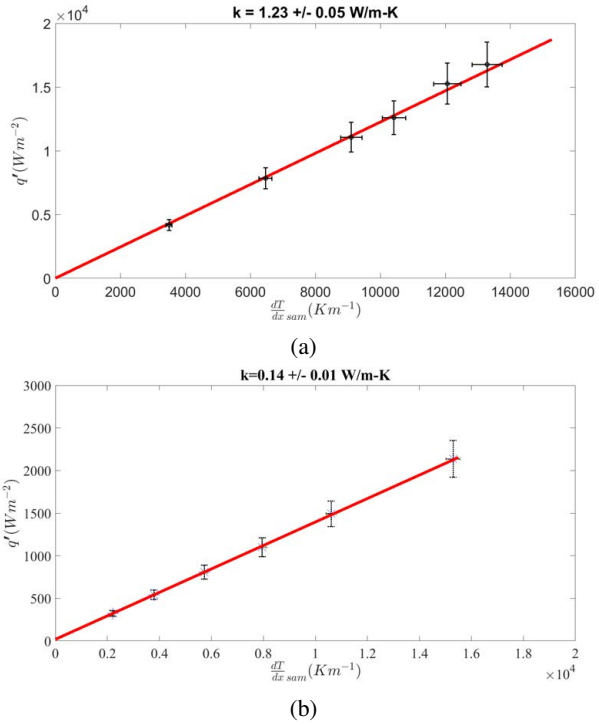

Fig. 13: Characterizing thermal conductivity of the (a) Arctic Blue thermal pad (b) silicone pad and using the reference bar method. The heat flux is linearly proportional to the temperature gradient in the sample by the thermal conductivity.

Appendix C: Characterizing thermal pad thermal conductivity using cross-plane technique

The thermal conductivity of the silicone rubber pad (from McMASTER-CARR) and Arctic Blue thermal pad (from ARCTIC) were characterized using a modified version of the ASTM-D5470 reference bar method using IR microscope for thermal measurements [17]. The sample (silicone pad or Arctic Blue) of unknown thermal conductivity are placed between two reference layers of known thermal conductivity. The entire reference-sample-reference stack is placed between a heater and heat sink. Six different steady state thermal images are taken by changing the heater power level and the temperature gradient as a function of heat flux through the reference layers is calculated. Finally, as shown in Fig 13a and Fig. 13b, a linear curve was fit in order to obtain the slope and hence the thermal conductivity: $k_{silicone-pad} = 0.14 \pm 0.01$ $\mathrm{Wm^{-1}K^{-1}}$ and $k_{arctic-blue-pad} = 1.14 \pm 0.05$ $\mathrm{Wm^{-1}K^{-1}}$.

References

[1] H. M. Bird, "Approaches to Electronic Miniaturization," *IEEE Transactions on Components Packaging and Manufacturing Technology Part A*, vol. 18, no. 2, pp. 274–278, 1995.

[2] R. L. Henry, R. K. Scal, and G. Shapiro, "New Techniques for Electronic Miniaturization," *Proceedings of the IRE*, vol. 38, no. 10, pp. 1139–1145, 1950.

[3] H. Iwai, "(Gordon E. Moore Award) Impact of Micro-/Nano-Electronics, Miniaturization Limit, and Technology Development for the Next 10 Years and After," *ECS Transactions*, vol. 102, no. 4, pp. 81–95, 5 2021.

[4] Y. Zhou, S. Wu, Y. Long, P. Zhu, F. Wu, F. Liu, V. Murugadoss, W. Winchester, A. Nautiyal, Z. Wang, and Z. Guo, "Recent Advances in Thermal Interface Materials," pp. 4–24, 3 2020.

[5] C. Deppisch, T. Fitzgerald, A. Raman, F. Hua, C. Zhang, P. Liu, and M. Miller, "The material optimization and reliability characterization of an indium-solder thermal interface material for CPU packaging," *JOM*, vol. 58, no. 6, pp. 67–74, 2006.

[6] X. Hu, L. Jiang, and K. E. Goodson, "Thermal characterization of eutectic alloy thermal interface materials with void-like inclusions," in *Annual IEEE Semiconductor Thermal Measurement and Management Symposium*, vol. 20. IEEE, 2004, pp. 98–103.

[7] R. Viswanath, M. Group, and I. Corp, "Thermal Performance Challenges from Silicon to Systems," *Intel Techology Journal Q3*, pp. 1–16, 2000. [Online]. Available: http://citeseerx.ist.psu.edu/viewdoc/summary?doi=10.1.1.14.8322

[8] V. Khuu, M. Osterman, A. Bar-Cohen, and M. Pecht, "Effects of temperature cycling and elevated temperature/humidity on the thermal performance of thermal interface materials," *IEEE Transactions on Device and Materials Reliability*, vol. 9, no. 3, pp. 379–391, 9 2009.

[9] J. Due and A. J. Robinson, "Reliability of thermal interface materials: A review," in *Applied Thermal Engineering*, vol. 50, no. 1, 2013, pp. 455–463.

[10] D. DeVoto, J. Major, P. Paret, and Institute of Electrical and Electronics Engineers, "Degradation Characterization of Thermal Interface Greases," *16th IEEE Intersociety Conference on Thermal and Thermomechanical Phenomena in Electronic Systems (ITherm)*, 2017.

[11] S. N. Paisner, M. Touzelbaev, G. Refai-Ahmed, and Y. Yang, "New developments for a no-pump-out high-performance thermal grease," in *2010 12th IEEE Intersociety Conference on Thermal and Thermomechanical Phenomena in Electronic Systems, ITherm 2010*, 2010.

[12] C. P. Chiu, B. Chandran, M. Mello, and K. Kelley, "An accelerated reliability test method to predict thermal grease pump-out in flip-chip applications," *Proceedings - Electronic Components and Technology Conference*, pp. 91–97, 2001.

[13] I. M. Nnebe and C. Feger, "Drainage-induced dry-out of thermal greases," *IEEE Transactions on Advanced Packaging*, vol. 31, no. 3, pp. 512–518, 2008.

[14] A. Gowda, D. Esler, S. Tonapi, K. Nagarkar, and K. Srihari, "Voids in thermal interface material layers and their effect on thermal performance," in *Proceedings of 6th Electronics Packaging Technology Conference, EPTC 2004*, 2004, pp. 41–46.

[15] H. Carlton, D. Pense, and D. Huitink, "Thermomechanical Degradation

of Thermal Interface Materials: Accelerated Test Development and Reliability Analysis," *Journal of Electronic Packaging, Transactions of the ASME*, vol. 142, no. 3, 9 2020.

[16] C. A. Schneider, W. S. Rasband, and K. W. Eliceiri, "NIH Image to ImageJ: 25 years of image analysis," pp. 671–675, 7 2012.

[17] A. Gaitonde, A. Nimmagadda, and A. Marconnet, "Measurement of interfacial thermal conductance in Lithium ion batteries," *Journal of Power Sources*, vol. 343, pp. 431–436, 2017.